Preliminary Remote Sensing Investigation towards Geological Mapping in Northwest Libya

N. M. Saadi, K. Watanabe and H. Mizunaga
Department of Earth Resources Engineering, Kyushu University, 744 Motooka, Nishi-Ku, Fukuoka 819-0395, Japan, Saadi-n@mine.kyushu-u.ac.jp

Abstract

This study presents a detailed analysis based on digital process of optical Landsat Enhanced Thematic Mapper Plus (ETM+) and radar (C-band Synthetic Aperture Radar (ERS-2 SAR)) remote sensing data, and digital elevation model (DEM) extracted from topographic maps (1:50,000) to evaluate their efficiency for geological mapping in the Jifara Plain of northwest Libya. Lithological and structural units were distinguishable based on their topographic form and spectral properties. GIS and remote sensing-based methods were used to integrate all raster and vector results extracted from multiple geoscientific data types. The results discriminated eighteen lithological units were plotted in the geological map defined by the new boundaries. The dominant extracted lineaments tend to run in the NW-SE direction. Analysis and interpretation of the extracted lineaments provided information about the tectonic evolution of the study area. Field work was done for ground-based verification of remote sensing data.

Keywords : ETM+, DEM, ERS-2 SAR, Image processing, Geological mapping

1. Introduction

The sensors of remote sensing satellites can image geological features based on their spatial and spectral resolution (Masoud and Koike, 2006 ; Yang et al., 2007; Saadi and Watanabe, 2008). Several analysis and image processes were implemented in this study to enhance the visual interpretation and discrimination of different lithological units and the extraction of geological lineaments in the Jifara Plain of northwest Libya. The Jifara Plain has been the subject of numerous geological studies by different geologists in the 1940s, 1960s, and 1970s (Lipparini, 1940; Jordi and Lonfat, 1963; Christie, 1966 ; El Hinnawy and Cheshitev, 1975; Antonovic, 1977).

In this study, an attempt has been made to use diverse data sets such as Landsat ETM+ image, ERS-2 SAR, and DEM data for further geological investigations. Remote sensing data processing and interpretation was applied in this study in three phases. During the first phase, distinguishing the spatial distribution of basalt flows, basalt cones and phonolite intrusions by integrating ETM+ thermal infrared (TIR) and visible-near infrared (VNIR) bands and ERS-2 SAR C-band (Leech et al., 2003; Cengiz et al., 2006; Pereira et al., 2008). The Intensity-Hue-Saturation (IHS) transformation was used to fuse the optical and radar data (Mather, 2004). Basically, data fusion techniques used to improve the spatial and spectral resolution of remote sensing data by combining multi-satellite images (Jensen, 1996; Solberg, 2006). In the second phase, a series of landform interpretation experiments was conducted on the ETM+ images by using different False Color Composites (FCC) (Gibson and Power, 2000; Hoffman and Markman, 2001) and Principal Component Analysis (PCA) (Chen , 2006) for further lithological units recognition. In the third phase, extracting and mapping geological lineaments using DEM data extracted from topographic maps (1:50,000). The DEM were used to overcome the obscuring effects of artificial features in order to extract geological lineaments (Gloaguen et al., 2007 ; Demirkesen, 2008). Calculating and interpreting DEM derivatives including shaded relief maps and slope maps. The manual extraction criteria for the lineaments were based on photographic characteristics, including shape and geomorphologic features.

Field work was done to confirm the remote sensing implications by identifying lithological boundaries and determining the artificial lines, which could eventually generate edges on the remote sensing data.

The results discriminated eighteen rock units and sediments. These units were identified and plotted in the new geological map defined by new boundaries. More than six hundred geological lineaments were discriminated in the study area. The segregation of extracted lineaments in to groups based on the age of the geological formations provided information about the tectonic structure of the study area.

2. Geological Setting

The study area lies in the northwestern part of Libya, bounded by longitudes 12°10′ E to 13°55′ E and latitudes

31°50′ N to 32°55′ N. It covers a surface area of approximately 20000 km2. It can be distinguished into three main Geomorphological units. These units are known as the Jifara Plain, the Scarp, and the Plateau. The Jifara Plain is bounded from the north by the Mediterranean Sea and from the south by the scarp of Jabal Nafusah (Conant and Goudarzi, 1967). The Jabal Nafusah runs approximately in an east-west direction from the Mediterranean Sea and westwards to beyond the Libyan border. It overlooks the Jifara Plain and rises above sea level for an elevation ranges from 500 to 700 meters (El Hinnawy and Cheshitev, 1975). The Plateau is a Questa made mainly of hard and resistant dolomitic limestone of Upper Cretaceous age. The southeast area is covered by basalt sheets with scattered black hills made of phonolite and basalt (Antonovic, 1977; Zivanovic, 1977).

The study area contains exposures of sedimentary rocks ranging in age from Triassic to Quaternary. The study area is characterized by uplifts, subsidences and block faulting (Miller, 1971; El Hinnawy and Cheshitev, 1975; Saadi et al., 2009).

3. Data Processing

The south region of the study area covered by basalt sheets with scattered black hills made of phonolite and basalt. The ETM+ TIR band was tested to discriminate multi volcanic rocks on the basis of an expected difference in emissivity with VNIR band-ratio (NIR/G) because of their higher spatial resolution and ERS-2 C band for discriminating different volcanic rocks on the basis of their surface roughness. For fusing images, the IHS–RGB transformation was used to display spectral variations in a single RGB color combination image. The hue defines the color based on the dominant wavelength; the saturation defines the purity of the color; the intensity defines the brightness (Mather, 2004). Hence, the multi-spectral information in the ETM+ data is used to define the hue and saturation while the radar data are used to define the intensity (Fig. 1).

Several false color composite (FCC) images using Landsat ETM+ were created to improve the visual interpretation. These band combinations included RGB-742, RGB-234, RGB-456, RGB-467, and RGB-367. The optimum index factor (OIF) method (Chavez et al., 1982) was used to calculate the variance of different band combinations. The VNIR bands have the advantage of preserving morphological features and displaying different lithological units in vivid different colors. Mid infrared band can be used to distinguish clay units because clay minerals have a significant absorption feature within this band (Sabins, 1997). Near infrared band is effective in mapping iron oxides because these minerals have high reflectance within this band (Abdelsalam et al. 2000). The bands MIR-NIR-G are effective in geological mapping in arid regions because of lack of vegetation (Fig. 2). Additionally, the first three PCA of ETM+ band-combinations were used to show the lithological units with vivid colors.

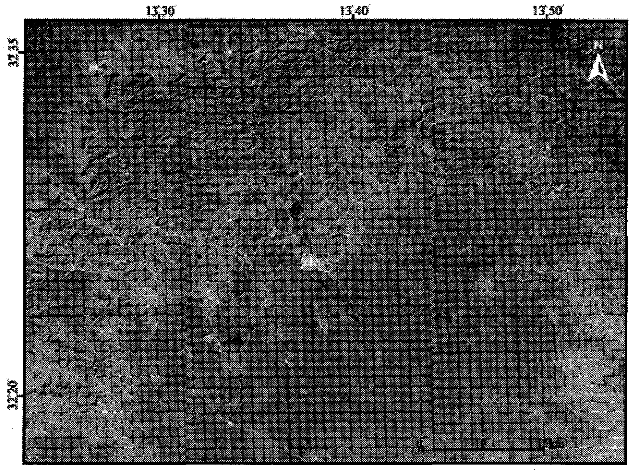

Fig. 1. Partial frame of RGB-IHS

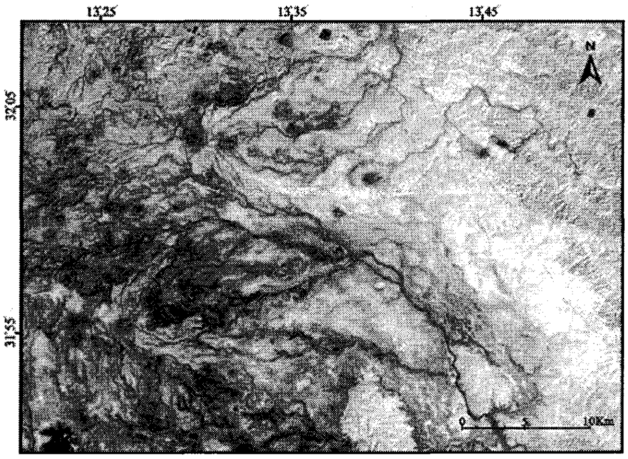

Fig. 2. Partial frame of FCC MIR-NIR-G

DEM constructed from topographic contour maps (1:50,000) (S.P.L.A.J., 1979). The contour interval of the topographic maps was 20 m, with supplementary contours at 10 m intervals. The produced DEM has a horizontal resolution of 20 m and a vertical resolution of 5 m. DEM data have been used to detect and map geological lineaments by calculating and interpreting DEM derivatives, including shaded relief maps and slope maps. In shaded relief maps, we experimented with the evaluation of an incoming illumination that is perpendicular to the prevailing trend of lineaments in the study area. According to the old geologic map of the study area, the prevailing lineaments trend in the NW-SE directions (I.R.C., 1975). Therefore, low incoming solar radiation from the NE-NNE was tested to mitigate azimuth-biasing effects and enhance the visual detection of linear features in the dominant trend. A low sun-elevation angle (20° to 30°) was used for lineament detection in all directions (Fig. 3). Slope map was created using a quadratic fitted to a 3×3 kernel. The output image contains slope values that range from 0° (flat terrain) to 90° (vertical terrain) (Fig. 4). Topographic lineaments can be distinguished by their elevation difference from the surrounding terrain. These elevation changes can be represented as changes in colors in the slope map.

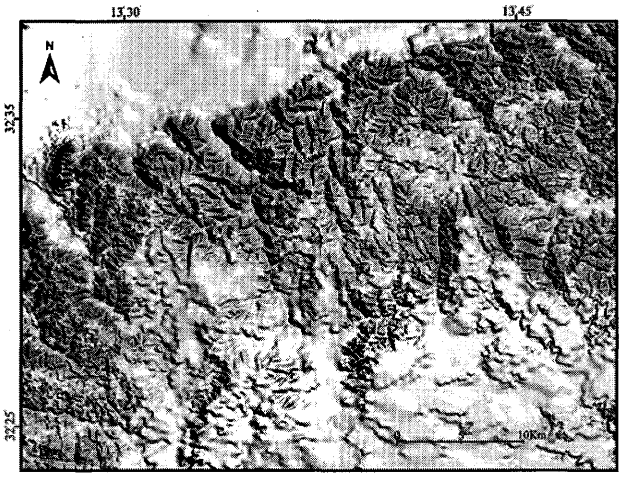

Fig. 3. Partial frame shaded relief map

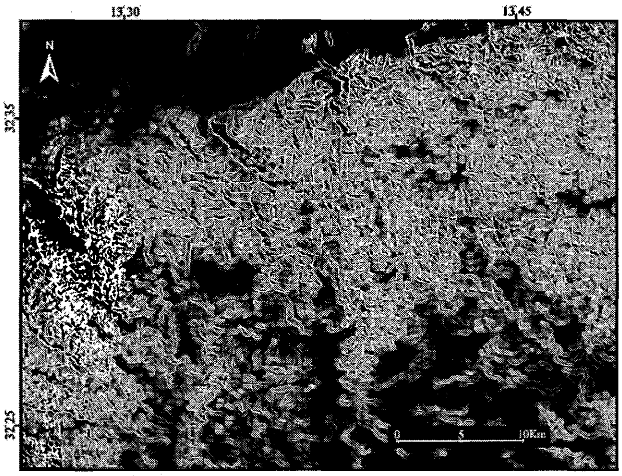

Fig. 4. Partial frame slope map

4. Results and Discussion

The general results indicate that ETM+, ERS-2, and DEM data are able to discriminate different rock units and extract geological lineaments in the Jifara Plain. The following eighteen rock and sediments units were identified and plotted on the new lithological map (Fig.5).

1- Al Aziziyah Formation: This unit consists mainly of bedded limestone characterized by its dark grey color. This formation was recognized using FCC image RGB-MIR, NIR, and G.
2- Abu Shaybah Formation: This unit consists of sandstone alternating with layers of clays and scattered limey bands. This formation was recognized using fused image RGB-TIR, VNIR, and ERS-2 C band.
3- Abu Ghaylan Formation: This unit consists mainly of limestone. This formation was recognized using FCC image RGB-NIR, TIR, and MIR.
4- Bir al Ghanam Formation: This unit consists mainly of white to grey system. This formation was recognized using fused image RGB-TIR, VNIR, and ERS-2 C band.
5- Takbal Formation: This unit consists of limestone with clayey and marly intercalations. This formation was recognized using FCC image RGB-NIR, TIR, and MIR.
6- Sidi as Sid Formation: This unit consists of limestone and marl. This formation was recognized using FCC image RGB-NIR/G, MIR and TIR.
7- Nalut Formation: This unit consists of limestone and dolomitic limestone. This formation was recognized using FCC image RGB-NIR/G, MIR and TIR.
8- Qasr Tigrinnah Formation: This unit consists of a succession of soft marls and white to rosy limestone. This formation was recognized using FCC image RGB-MIR, NIR, and G.
9- Mizda Formation: This unit consists of marl, shale, and chalky limestone. This formation was recognized using FCC image RGB-NIR, TIR, and MIR.
10- Al Khums Formation: This unit consists of limestone and algal limestone. This formation was recognized using FCC image RGB-NIR/G, MIR and TIR.
11- Volcanic rocks: This unit consists of phonolite and trachyte intrusions, basalt cones, and basalt flows. This formation was recognized using fused image RGB-TIR, VNIR, and ERS-2 C band.
12- Quaternary: Five types of Quaternary sediments were discriminated and mapped: Qasr Al Haj Formation, Jifara Formation, Sebkha sediments, Fluvio-eolian sediments and Eolian deposits. These sediments were recognized using FCC image RGB-NIR/G, MIR and TIR, RGB-MIR, NIR, and G, and fused image RGB-TIR, VNIR, and ERS-2 C band.

The RGB-TIR, VNIR, and ERS-2 C band and RGB-MIR, NIR, and G images permitted the successful identification of lithological units in the study area.

Structurally, the DEM data identified 641 geological lineaments (Fig. 5). The low illumination angle was most suitable for detecting lineaments. Lineaments extracted from the DEM have different trends, but the main trend is NW-SE, parallel to the main tectonic line of the Jabal Uplift. The NE-SW lineaments represent a secondary trend. Lineaments extracted from the DEM were divided into six groups on the basis of the ages of the surrounding geological formations. Lineaments in the Upper Triassic rocks trend dominantly NW-SE. Lineaments in the Upper Triassic - Middle Jurassic rocks trend dominantly NW-SE. The prevailing trend of the Middle Jurassic rock lineaments is NE-SW. Lineaments in the Upper Cretaceous rocks are dominantly NW-SE. Lineaments in the Tertiary rocks are mostly NW-SE, with the NE-SW direction being subordinate. Lineaments in

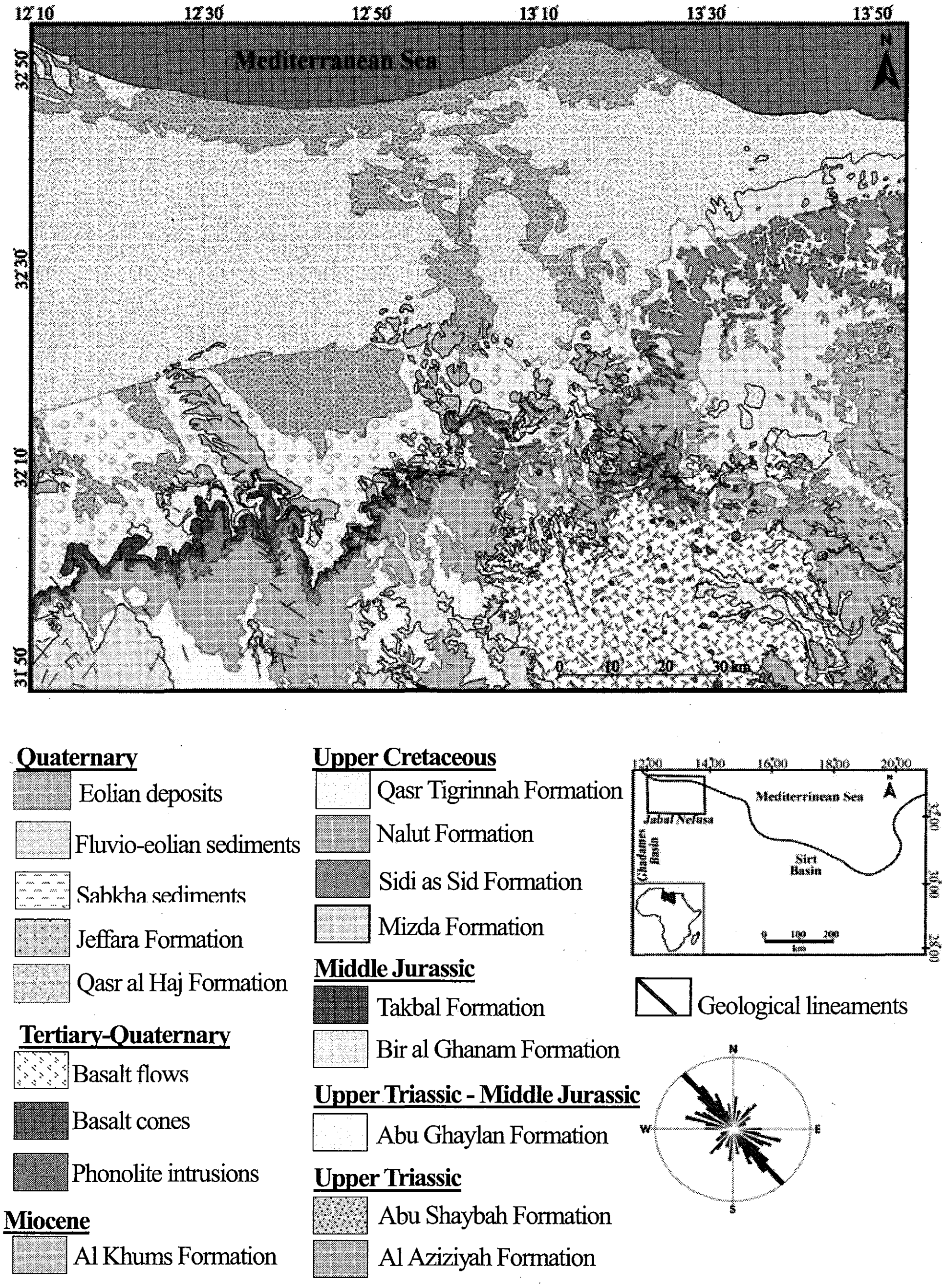

Fig. 5. Geologically interpreted map of the study area

Quaternary sedimentary units trend dominantly NW-SE. Analysis of extracted lineaments was based on the principle of cross-cutting relationships (Rowland and Duebendorfer, 1994). Analysis and interpretation of the DEM results indicates that the different lengths of the NW-SE lineaments in the Upper Cretaceous rocks probably indicate reactivated faulting. Lithologically, the arrangement of phonolite hills and basalt cones in lines parallel to the dominant lineament trends (NW-SE) indicates that the volcanic activity is related to the tectonic activity of the Jabal Uplift.

Acknowledgements

This work was supported in part by the Japanese Society for the Promotion of Science (JSPS) and by the Global-Centre of Excellence in Novel Carbon Resource Sciences.

References

1) Abdelsalam, M.G., Stern, R.J., and Berhane, W.G., 2000. Mapping gossans in arid regions with Landsat TM and SIR-C images: the Beddaho alteration zone in northern Eritrea. Journal of African Earth Sciences, 30 (4), 903–916.
2) Antonovic, A., 1977. Geological map of Libya, explanatory booklet, sheet Mizdah NH 33-1," I.R.C., Tripoli.
3) Cengiz, O., Sener, E. and Yagmurlu, F., 2006. A satellite image approach to the study of lineaments, circular structures and regional geology in the Golcuk Crater district and its environs (Isparta, SW Turkey). Journal of Asian Earth Sciences, 27 (2), 155_163.
4) Chavez, P.S., Berlin, G.L., and Sowers, L.B., 1982. Statistical methods for selecting Landsat MSS ratios. Journal of Applied Photographic Engineering, 8, 23–30.
5) Chen, F.W., 2006. Satellite-based precipitation retrieval using neural networks, principal component analysis, and image sharpering. In: C.H. Chen, ed. Signal and image processing for remote sensing. Boca Raton, FL: CRC Press, 233–266.
6) Christie, A.M., 1966. Geology of Gharyan Area, Tripolitania, Libya. Ministry of Industry, Geological Section Bulletin, No. 5, Tripoli.
7) Conant, L.C. and Goudarzi, G.H., 1967. Stratigraphic and tectonic framework of Libya. AAPG Bull., vol. 51, no. 5, pp. 719–730.
8) Demirkesen, A.C., 2008. Digital terrain analysis using Landsat-7 ETM+ imagery and SRTM DEM: A case study of Nevsehir province (Cappadocia), Turkey. Int. J. Remote Sens., vol. 29, no. 14, pp. 4173–4188.
9) El Hinnawy, M. and Cheshitev, G, 1975. Geological map of Libya. Explanatory booklet, sheet Tarabulus NI 33_13. Industrial Research Centre, Tripoli.
10) Gibson, P.J. and Power, C.H., 2000. Introductory remote sensing. Digital image processing and applications. London: Routledge.
11) Gloaguen, R., Marpu, P.R. and Niemeyer, I., 2007. Automatic extraction of faults and fractal analysis from remote sensing data. Nonlinear Proc. Geoph., vol. 14, no. 2, 131–138.
12) Hoffman, R.R. and Markman, A.B., eds. 2001. Interpreting remote sensing imagery: human factors. Boca Raton, FL: Lewis Publishers.
13) Industrial Research Centre (I.R.C), 1975. Geological map of Libya, 1:250,000, sheet: Tarabulus, Tripoli-Libya.
14) Jensen, J.R., 1996. Introductory digital image processing. Prentice Hall Series in Geographic Information Science. 2nd Ed., New Jersey: Prentice Hall Publishers.
15) Jordi, H.A. and Lonfat, F., 1963. Stratigraphic subdivision and problems in Upper Cretaceous–Lower Tertiary deposits in Northwestern Libya. In Saharan Symposium Tripoli, Petrol. Expl. Soc. of Libya, pp. 114–122.
16) Leech, D.P., Treloar, P.J., Lucas, N.S. and Grocott, J., 2003. Landsat TM analysis of fracture patterns: a case study from the Coastal Cordillera of northern Chile. Int. J. Remote Sens., vol. 24, no. 19, pp. 3709–3726.
17) Lipparini, T., 1940. Tettonica e geomorfologia della Tripolitania. Bulletin of the Geological Society of Italy, Roma 59, 221-301.
18) Masoud, A. and Koike, K., 2006. Tectonic architecture through Landsat-7 ETM+/SRTM DEM derived lineaments and relationship to the hydrogeologic setting in Siwa region, NW Egypt. Journal of African Earth Sciences, 45 (4–5), 467–477.
19) Mather, P.M., 2004. Computer Processing of Remotely-Sensed Images. 3rd ed. Chichester, U.K, Wiley.
20) Miller, V.C., 1971. A Preliminary Investigation of the Geomorphology of the Jebel Nefusa. In Symp. Geol. of Libya, Univ. of Libya, Tripoli, pp. 365–385.
21) Pereira, A. J.S.C., Victória, S., Vicente, A.M.P. and Neves, L.J.P.F., 2008. Structural lineaments in a volcanic island evaluated through remote sensing techniques. The case of Santiago Island (Cape Verde). International Geoscience and Remote Sensing Symposium (IGARSS), art. No. 4423127, 1632_1635.
22) Rowland, S.M. and Duebendorfer, E.M., 1994. Structural analysis and synthesis: 2nd edition. Blackwell Scientific Publications, Palo Alto.
23) Saadi, N.M. and Watanabe, K., 2008. Lineaments extraction and analysis in Eljufra area, Libya. Journal of Applied Remote Sensing, 2, 023538.
24) Saadi, N.M., Aboud, E. and Watanabe K., 2009. Integration of DEM, ETM+, geologic, and magnetic data for geological investigations in the Jifara Plain,

Libya, IEEE Transactions on Geoscience and Remote Sensing, Vol. 47, No. 10, pp. 3389-3398.

25) Sabins, F., 1997. Remote sensing principles and interpretation. New York: W.H. Freeman Company.

26) Solberg, A.H.S., 2006. Data fusion for remote sensing applications. In: C. H. Chen, ed. Signal and image processing for remote sensing. Boca Raton, FL: CRC Press, 515–537.

27) S.P.L.A.J., 1979. Topographic map of Libya, 1:50,000. Polservice-Geokart, Poland.

28) Yang, J.M., Zhang, Y.J. and Yao, F.J., 2007. Lithology identification of the Weiya complex by means of ETM+ remote sensing. Acta Petrologica Sinica, 23(10), 2397–2402.

29) Zivanovic, M., 1977. Geological map of Libya. Explanatory booklet, sheet Bani Walid NH 33-2. Industrial Research Centre, Tripoli.